Journal of Solid State Chemistry **163,** 406–411 (2002)
doi:10.1006/jssc.2001.9413, available online at http://www.idealibrary.com on IDEAL®

Nuclear and Magnetic Structure of Layered $LiFe_{1-x}Co_xO_2$ ($0 \leq x \leq 1$) Determined by High-Resolution Neutron Diffraction

N. Douakha,*,† M. Holzapfel,‡,§ E. Chappel,*,[1] G. Chouteau,* L. Croguennec,¶ A. Ott,§ and B. Ouladdiaf‖

*Grenoble High Magnetic Field Laboratory, CNRS/MPI-FKF, 25 avenue des Martyrs, BP 166, 38042 Grenoble, France; †LPG, BP 401, Guelma 24000, Algerie; ‡Laboratoire d'Electrochimie et de Physicochimie des Matériaux et des Interfaces, LEPMI-INPG, 1130 rue de la piscine, BP 75, 38402 St. Martin d'Hères, France; §Institut für Anorganische Chemie, Universität Tübingen, Auf der Morgenstelle 18, 72076 Tübingen, Germany; ¶ICMCB-CNRS and ENSCPB, 87, Avenue du Dr A. Schweitzer, 33608 Pessac cedex, France; and ‖Institut Laue Langevin, BP 156, 38042 Grenoble Cedex 9, France

Received July 31, 2001; in revised form September 26, 2001; accepted September 28, 2001

Mixed lithium–transition metal oxides $LiFe_{1-x}Co_xO_2$ ($0 \leq x \leq 1$) have been studied by powder neutron diffraction in the temperature range 1.5–100 K and at room temperature. The low-temperature data analysis of the high-flux neutron diffraction patterns reveals an antiferromagnetic arrangement with a propagation vector $k = [0\,0\,\frac{1}{2}]$. The value obtained for the magnetic moment of Fe^{3+} ions at 1.5 K, $\mu_{Fe^{3+}} = 3.9\,\mu_B$, is in good agreement with the value deduced from magnetization data and is also consistent with the high spin state of Fe^{3+} ion. The crystallographic structure was determined by both X-ray and high-resolution neutron diffraction measurements. © 2002 Elsevier Science (USA)

Key Words: **layered magnetic oxides; high-resolution neutron diffraction; magnetic structure; materials for lithium batteries.**

1. INTRODUCTION

The layered $LiMO_2$ oxides (M = Co, Ni, Mn, Fe) with the α-$NaFeO_2$-type structure are among the most promising positive electrode materials for rechargeable lithium-ion batteries. $LiCoO_2$ is the most often used material, thanks to its high structural stability upon long-range cycling, its good power rate, its low self-discharge, its relatively easy preparation, and its thermal stability in the battery. Nevertheless, due to the high price and toxicity of cobalt, $LiCoO_2$ is not a good candidate as positive electrode material in large batteries for electrical vehicles. $LiNiO_2$ shows a very high reversible capacity, but poor cycle life and small thermal stability in the delithiated state. Nevertheless, it should be noted that recent works have shown that partial substitution for nickel solves all these problems: indeed, Co (1), Mg (2), or Al (3) substitution for nickel improves the 2D character of the structure, the cycle life, and the thermal stability, respectively. Research has also been done with the aim of finding new attractive positive electrode materials. In the frame of these studies, layered $LiFeO_2$ compounds have also been widely studied (4–6). No reversible lithium deintercalation from the α-$NaFeO_2$-type structure could be achieved, whereas two $LiFeO_2$ forms with other structure types were successfully tested by Kanno *et al.*, at least for partial lithium deintercalation (7, 8). One of these electrochemically active $LiFeO_2$ phases crystallizes in a corrugated layered structure, isostructural to orthorhombic $LiMnO_2$. This $LiFeO_2$ phase was obtained using a hydrothermal reaction and it was found that the Li//$LiFeO_2$ cell exhibited good charge and discharge reversibility between 1.5 and 3.0 V vs Li/Li^+. Delmas *et al.* have suggested that for the α-$NaFeO_2$-type $LiFeO_2$, in contrast to what is observed for the Li(Ni,Fe)O_2 system, there is no structural constraint which contributes to the stabilization of the very unstable Fe^{4+} ions: lithium deintercalation, i.e., oxidation of Fe^{3+} to Fe^{4+}, is, therefore, difficult and probably requires too high voltage (9). Indeed, Delmas *et al.* have recently shown the effect of the structure on the relative stability of the various 3*d* cations' oxidation states, in the case of Li(Ni,Co)O_2 (10) and Li(Ni,Fe)O_2 systems (11): the compression of the FeO_6 octahedra in Li(Ni,Fe)O_2 stabilizes for instance the tetravalent state for iron upon oxidation. Due to its smaller size, partial cobalt substitution for iron is, therefore, also expected to promote reversible lithium deintercalation from the $LiFe_{1-x}Co_xO_2$ system upon oxidation.

Iron substitution in $LiCoO_2$ was initially achieved in a limited composition range ($0 \leq x < 0.3$) by Kobayashi *et al.* using a hydrothermal reaction at 300°C (12) and by Alcántara using a solid-state high-temperature reaction at 800°C (13). Using an indirect approach by Na^+/Li^+ ion-exchange, we succeeded in the preparation of the solid

[1] To whom correspondence should be addressed. Present address: MEMSCAP, 50 allée des Dauphins, 38330 St Ismier, France. Fax: + 334 76 52 55 81. E-mail: eric.chappel@memscap.com.

0022-4596/02 $35.00

solution $LiFe_{1-x}Co_xO_2$ in the whole composition range ($0 \leq x \leq 1$) and reported its structural, physicochemical, and electrochemical characterization (14). The high-field magnetic properties of these samples have been presented in a previous work (15). In the present study, we present the magnetic structure investigated for selected members of the solid solution $LiFe_{1-x}Co_xO_2$, using high-resolution neutron diffraction.

2. EXPERIMENTAL

Lithium–transition metal oxides $LiFe_{1-x}Co_xO_2$ ($0 \leq x \leq 1$) with different nominal compositions were prepared by Na^+/Li^+ ion-exchange reaction from $NaFe_{1-x}Co_xO_2$. The former were obtained by reacting the $NaFe_{1-x}Co_xO_2$ samples in an eutectic $LiCl/LiNO_3$ mixture, washing with methanol, and drying under vacuum. More details are given elsewhere (4, 14).

The parent solids, Na_2O_2 powder (95%, Fluka), Co_3O_4 (puriss. p.A., Merck), and Fe_2O_3 (carbonyl iron oxide, BASF), were thoroughly mixed with a slight excess of Na_2O_2 in an argon atmosphere. The powders were heated in air with intermittent grinding [described in detail in (14)].

Magnetic susceptibility was performed on a SQUID magnetometer (Quantum Design, MPMS) at 1 kOe between 4 and 200 K and on an extraction magnetometer up to 600 K at 20 kOe. High magnetic field measurements were performed at the Grenoble High Magnetic Field Laboratory facilities using resistive magnets.

Neutron diffraction measurements were carried out using the high-resolution two-axis diffractometer D2B at the Institute Laue-Langevin in Grenoble (France). In order to refine the crystallographic structure, neutron powder diffraction patterns were collected at room temperature using D2B with a wavelength $\lambda = 1.594$ Å. Low-temperature patterns were also collected for samples with $x = 0$, 0.2, and 1. The detector of D2B covers an angular range of 160° in 2θ with a step width of $\delta(2\theta) = 0.05°$. The complete diffraction patterns were measured several times at each temperature in order to obtain good statistics. To study the thermal evolution of the magnetic structure, the high-flux powder diffractometer D1B was used with a neutron wavelength $\lambda = 2.52$ Å. D1B is equipped with a position-sensitive detector composed of 400 cells and covers 80° in 2θ. Rietveld refinement of the magnetic and nuclear structures at different temperatures was performed using the FULLPROF program (16).

3. RESULTS AND DISCUSSION

3.1. X-Ray and Magnetic Measurements

In our previous work we have already reported the results of the X-ray diffraction and magnetization measurements (14, 15). The XRD patterns of all the $LiFe_{1-x}Co_xO_2$ samples were characteristic of the α-$NaFeO_2$-type structure (17–21) and could be indexed on the basis of a rhombohedral unit cell, using the R-3m space group.

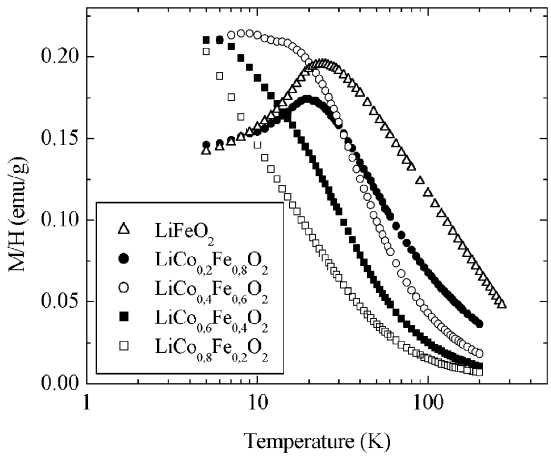

FIG. 1. Temperature dependence of M/H for $LiFe_{1-x}Co_xO_2$ with $x = 0$, 0.2, 0.4, 0.6, and 0.8.

The typical temperature dependence of M/H measured from 5 to 300 K is shown for $LiFe_{1-x}Co_xO_2$ in Fig. 1. For $x \leq 0.4$, an anomaly around 20 K indicates an antiferromagnetic ordering. Another important feature is that the temperature at which this maximum occurs decreases with increasing cobalt content (x). For $x = 0$, 0.2, and 0.4, the Néel temperature is 21, 20, and 8 K respectively. From the temperature dependence of H/M in the high-temperature regime (15), a positive θ Weiss temperature was observed for all samples, which indicates a predominance of ferromagnetic interactions.

In layered $LiFeO_2$ spin–flop transition and saturation have been observed by the high-field magnetization measurements at 4 K around 65 and 200 kOe, respectively (15). Considering the magnetization at saturation and the Curie constant of different $LiFe_{1-x}Co_xO_2$ samples, it has been concluded that the Fe^{3+} ions are in the high spin state ($t_{2g}^3 e_g^2$) with $S = \frac{5}{2}$ and the Co^{3+} ions are in the low spin state ($t_{2g}^6 e_g^0$) with $S = 0$, in good agreement with the values estimated by other workers (23, 24). It should be noted that no spontaneous magnetization has been observed, which indicates the absence of ferromagnetic impurities like Fe_3O_4 or γ-Fe_2O_3.

From the magnetic measurements described before, and in agreement with the Goodenough, Kanamori, and Anderson (GKA) rules, an A-type AF structure has been proposed (15). We have undertaken a neutron diffraction study of $LiFe_{1-x}Co_xO_2$ at low temperature in order to confirm unambiguously the real nature of the magnetic structure.

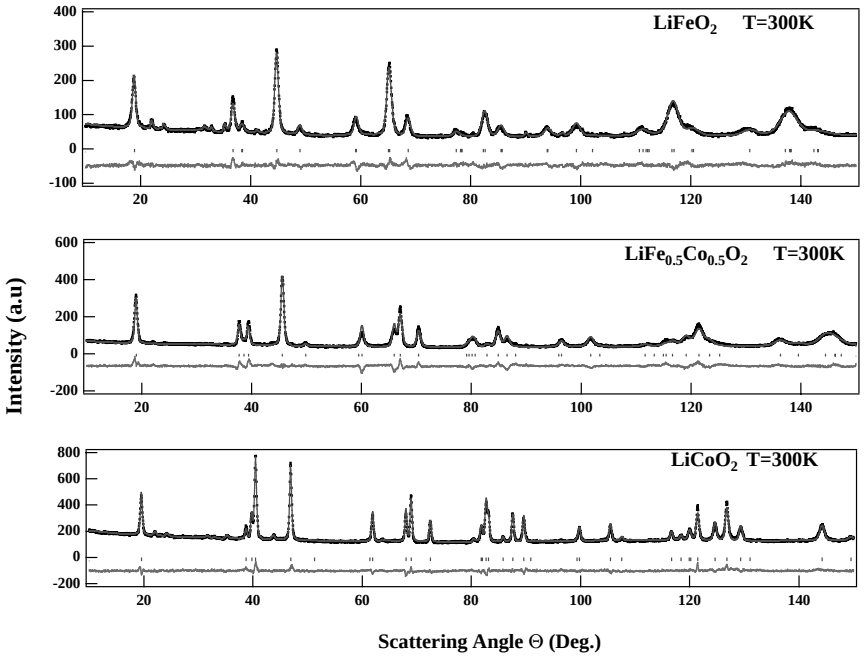

FIG. 2. High-resolution powder neutron diffraction patterns obtained at 300 K for $LiFeO_2$, $LiFe_{0.5}Co_{0.5}O_2$, and $LiCoO_2$. The full curves are the calculated patterns; the lower curves show the difference between observation and calculation.

3.2. Neutron Powder Diffraction Study

The neutron diffraction patterns collected in the paramagnetic state at 300 K for $LiCoO_2$, $LiFe_{0.5}Co_{0.5}O_2$, and $LiFeO_2$ are shown in Fig. 2. The patterns are characteristic of α-$NaFeO_2$-type structure. Small reflections due to an impurity phase are observed for some samples (this phase could not be identified further). All the other diffraction lines can be indexed in the $R\bar{3}m$ space group. As it has been argued before (14), a partial disorder of Fe^{3+} ions in the lithium planes implies a partial occupation of the metal planes by lithium. Indeed, no iron excess, but iron–lithium cationic mixing was considered, in good agreement with the high lithium excess used during the synthesis and with the results of the chemical analysis. Rietveld refinement was, therefore, performed assuming $(1-z)$Li and zFe in 3*a*-(000) and $y\mathrm{Co}^{3+}$, $(1-y-z)\mathrm{Fe}^{3+}$ and $z\mathrm{Li}^{+}$ in 3*b*-$(00\frac{1}{2})$ and $2\mathrm{O}^{2-}$ in 6*c*-positions (00*z*). The oxygen atomic position *z*, the Debye–Waller factors, and the atomic occupancies were refined. The results, which are in agreement with those deduced from X-ray diffraction, are summarized in Table 1. Figure 3 shows the variation of the lattice parameters with the cobalt content (*x*). The a parameter shows a linear variation while *c* deviates from linearity.

Increasing cobalt content results in decreasing lattice parameters, in good agreement with a smaller size for the

TABLE 1
Crystal Parameters of $LiFe_{1-x}Co_xO_2$ at $T = 300$ K Obtained from the Refinement of the Neutron Data

x	*a* (Å)	*c* (Å)	*z*	Fe occupation	B (Å²)–Li	B (Å²)–Fe	B (Å²)–O	R_B (%)	χ^2
1	2.9557(4)	14.532(3)	0.2445(2)		2.4(2)	0.7(1)	0.6(1)	6.7	2.5
0.9	2.9416(2)	14.534(2)	0.2429(2)	0.87	2.1(2)	0.6(1)	0.6(2)	6.5	6
0.7	2.9124(2)	14.489(2)	0.2425(1)	0.69	2.3(2)	0.5(1)	0.6(2)	6.4	3.5
0.5	2.8846(3)	14.451(2)	0.2395(10)	0.48	2.2(2)	0.6(1)	0.7(2)	11	5
0.4	2.8723(4)	14.408(3)	0.2400(2)	0.37	2.1(2)	0.9(2)	0.6(1)	13	9
0.3	2.8597(3)	14.327(3)	0.2392(5)	0.33	2.1(2)	0.8(1)	0.4(2)	9	3
0.2	2.8351(4)	14.168(2)	0.2401(3)	0.19	1.8(2)	0.6(1)	0.5(1)	7	4.9
0.1	2.8264(2)	14.126(1)	0.2390(2)	0.07	2.0(2)	0.6(1)	0.6(1)	9	11
0.0	2.8151(2)	14.047(1)	0.2393(7)		1.8(2)	0.8(1)	0.6(2)	8	4.7

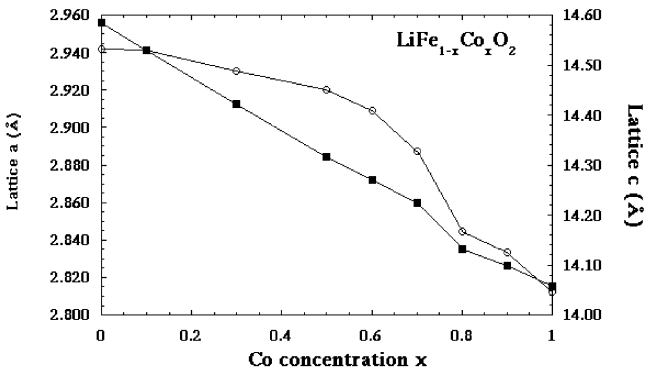

FIG. 3. Evolution of the lattice parameters with the Co concentration (x) at $T = 300$ K.

Co^{3+} ions versus the Fe^{3+} ones ($r(Co^{3+}) = 0.545$ Å and $r(Fe^{3+}) = 0.645$ Å). It should be noted that the decrease of the c-lattice parameter is larger than expected for a simple substitution of Co^{3+} for Fe^{3+}. Indeed, the iron-rich phases are characterized by iron–lithium cationic mixing between the slabs and the interslab spaces (note that perfect cationic ordering is known for $LiCoO_2$); a decrease of this disorder induces a large decrease of the MO_2 slab thickness (i.e., of the c-lattice parameter) due to the larger ionic radius of Li^+ versus Fe^{3+} and Co^{3+} ($r(Li^+) = 0.72$ Å).

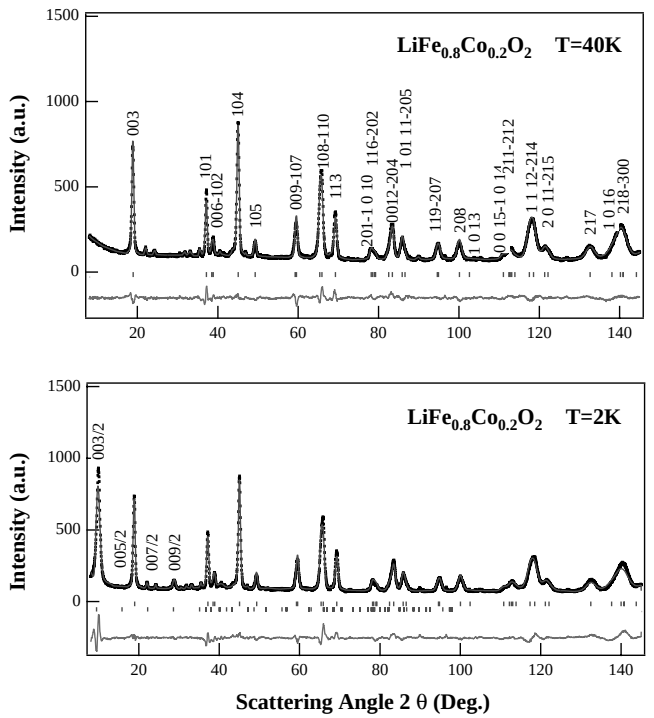

FIG. 4. High-resolution powder neutron diffraction patterns obtained at 40 K and 2 K for $LiFe_{0.8}Co_{0.2}O_2$. The full curves are the calculated patterns; the lower curves show the difference between observation and calculation.

In Fig. 4, we report the neutron diffraction patterns obtained at 40 K and 2 K for $LiFe_{0.8}Co_{0.2}O_2$. The data obtained at 40 K are similar to those collected at room temperature whereas the pattern collected at 2 K shows two additional peaks at $2\theta = 10^\circ$ and 30°, of magnetic origin. These peaks can be indexed by a propagation vector $k = [00\frac{1}{2}]$ leading to a magnetic cell two times larger than the crystallographic one with a doubling of the crystallographic cell along the c-axis. The two observed peaks are indexed as $(00\frac{3}{2})$ and $(00\frac{9}{2})$. The presence of the (001) reflections indicates that the magnetic moments are not oriented along the c-axis. The absence of the $(00\frac{5}{2})$ and $(00\frac{7}{2})$ reflections is a strong constraint in the determination of the magnetic structure. Indeed, the analysis of the magnetic structure factors requires that the Fe moments in one (001) layer are ferromagnetically ordered, while the coupling between adjacent layers is antiferromagnetic. The moment direction is perpendicular to the c-axis. Good agreement is obtained between observed and calculated patterns. The reliability factor for the magnetic structure is $R_M = 7\%$. The Fe magnetic moment deduced from the refinement reaches $m = 3.9\ \mu_B$/Fe, in agreement with the value obtained from magnetization data. The deduced magnetic structure is shown in Fig. 5. The neutron diffraction patterns collected on the high-flux diffractometer D1B confirm the magnetic structure deduced from the high-resolution patterns. Figure 6 shows the thermodiffractogram collected on D1B for the sample $LiFe_{0.8}Co_{0.2}O_2$. It indicates the appearance of the antiferromagnetic ordering around 20 K, the Néel temperature of the sample, and corresponds to the maximum of the susceptibility curve. The thermal dependence of the lattice parameters obtained from the neutron measurements is reported in Fig. 7. The lattice parameter a has an almost normal thermal expansion curve, while a net anomaly at low temperature is observed for the c parameter.

Very similar patterns are obtained at low temperatures for the $LiFe_{1-x}Co_xO_2$ samples within the concentration range $0 < x \leq 0.6$, the same magnetic peaks are observed but with a decreasing intensity with increasing x. On the other hand, the peak width increases with x, which indicates that the correlation length for the magnetic ordering decreases with Co concentration. The pattern collected at 2 K for the sample $LiFe_{0.4}Co_{0.6}O_2$ shows a broad peak, which is characteristic of a short-range ordering. For $x \geq 0.8$, no magnetic ordering was observed down to low temperatures.

The magnetic structure can be considered as a stacking of ferromagnetic layers perpendicular to the c-axis. The coupling between two adjacent layers is antiferromagnetic in agreement with GKA rules. Indeed, in layered $LiFeO_2$, 90° Fe–O–Fe intraplane bonds would give rise to ferromagnetic interactions. Conversely, the interplane interactions are expected to be antiferromagnetic (AF) since they take place either via 180° bonds including O $2p$ and Li $2s$ orbitals or

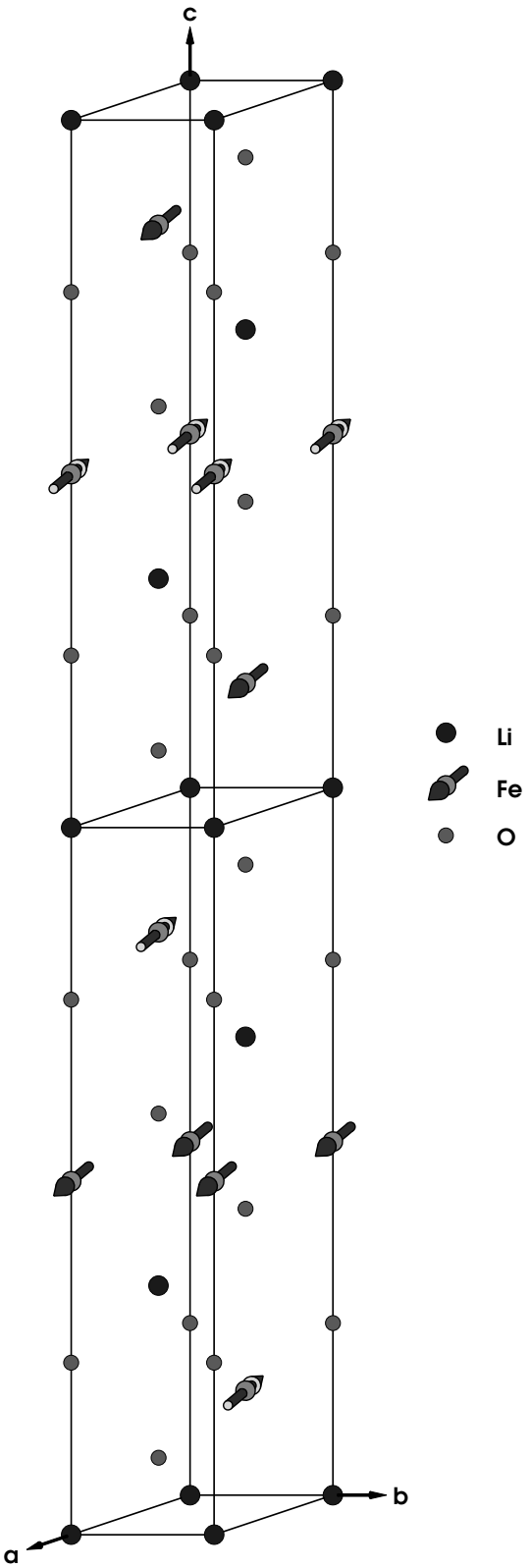

FIG. 5. Magnetic structure of $LiFe_{0.8}Co_{0.2}O_2$ at 2 K deduced from high-resolution powder neutron diffraction data.

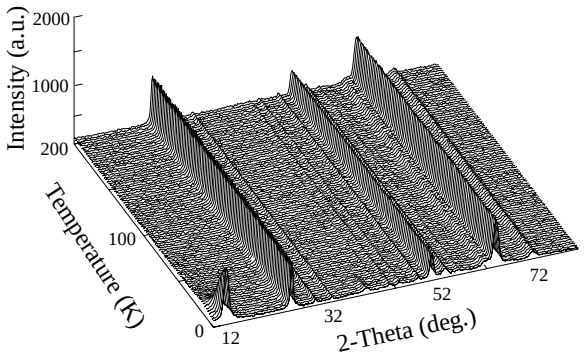

FIG. 6. Thermodiffractogram of $LiFe_{0.8}Co_{0.2}O_2$ obtained on the high-flux powder diffractometer D1B.

via other exchange paths including 90° bonds but with Li 2*s* orbitals: actually, virtual excitations through empty Li 2*s* and full O 2*p* orbitals can occur only if the Fe^{3+} spins are antiparallel, independently of the different bond angles.

4. CONCLUSION

Various layered $LiFe_{1-x}Co_xO_2$ compounds, synthesized by ion exchange, have been studied by means of high-resolution neutron diffraction. As for many hexagonal systems, $LiFeO_2$ is an A-type antiferromagnet with ferromagnetic iron layers antiferromagnetically coupled to each other. The spins lie in the Fe layers and the magnetic moment observed on the 3*d* site (3.9 μ_B/Fe^{3+}) is close to the one derived from susceptibility measurements (4.3 μ_B/Fe^{3+}). Introducing nonmagnetic Co ions leads to a dilution effect and only short-range correlations remain for $x > 0.6$, as evidenced by a diffuse magnetic peak at low temperatures. These results confirm the model predicted from high magnetic field measurements.

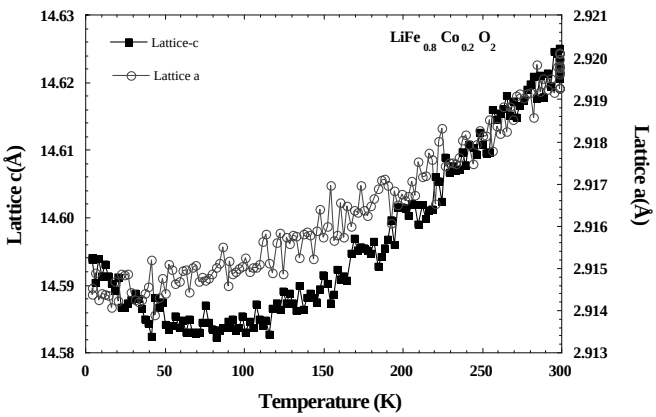

FIG. 7. Temperature dependence of the lattice parameters for $LiFe_{0.8}Co_{0.2}O_2$ deduced from the neutron data.

ACKNOWLEDGMENTS

The authors thank M. Basterreix from ICMCB (Bordeaux) for the preparation of some of the samples.

REFERENCES

1. A. Rougier, I. Saadoune, P. Gravereau, P. Willmann, and C. Delmas, *Solid State Ionics* **90,** 83 (1996).
2. C. Pouillerie, L. Croguennec, Ph. Biensan, P. Willmann, and C. Delmas, *J. Electrochem. Soc.* **147,** 2061 (2000).
3. T. Ohzuku, T. Yanagawa, M. Kouguchi, and A. Ueda, *J. Power Sources* **68,** 131 (1997).
4. B. Fuchs and S. Kemmler-Sack, *Solid State Ionics* **68,** 279 (1994).
5. T. Shirane, R. Kanno, Y. Takeda, M. Takano, T. Kamiyama, and F. Izumi, *Solid State Ionics* **79,** 227 (1995).
6. M. Tabuchi, C. Masquelier, T. Takeuchi, K. Ado, I. Matsubara, T. Shirane, R. Kanno, S. Tsutsui, S. Nasu, H. Sakaebe, and O. Nakamura, *Solid State Ionics* **90,** 129 (1996).
7. R. Kanno, T. Shirane, Y. Kawamoto, Y. Takeda, M. Takano, M. Ohashi, and Y. Yamaguchi, *J. Electrochem. Soc.* **143,** 2435 (1996).
8. R. Kanno, T. Shirane, Y. Inaba, and Y. Kawamoto, *J. Power Sources* **68,** 145 (1997).
9. G. Prado, Thesis, University of Bordeaux I, 2000.
10. I. Saadoune, M. Menetrier, and C. Delmas, *J. Mater. Chem.* **7,** 2505 (1997); I. Saadoune and C. Delmas, *J. Solid State Chem.* **136,** 8 (1998).
11. G. Prado, L. Fournès, and C. Delmas, *Solid State Ionics* **138,** 19 (2000); G. Prado, A. Rougier, L. Fournès, P. Willmann, and C. Delmas, *J. Electrochem. Soc.* **147,** 8 (2000).
12. H. Kobayashi, H. Shigemura, M. Tabuchi, H. Sakaebe, K. Ado, H. Kageyama, A. Hirano, R. Kanno, M. Wakita, S. Morimoto, and S. Nasu, *J. Electrochem. Soc.* **147,** 960 (2000).
13. R. Alcántara, P. Lavela, C. Pérez-Vicente, J. L. Tirado, J. Olivier-Fourcade, and J. C. Jumas, *Solid State Commun.* **115,** 1 (2000).
14. M. Holzapfel, C. Haak, and A. Ott, *J. Solid State Chem.* **156,** 470 (2001); M. Holzapfel, R. Schreiner, and A. Ott, *Electrochim. Acta* **46,** 1063 (2001).
15. E. Chappel, M. Holzapfel, G. Chouteau, and A. Ott, *J. Solid State Chem.* **154,** 451 (2000).
16. J. Rodriguez-Carvajal, *Physica B* **192,** 55 (1993).
17. H. J. Orman and P. J. Wiseman, *Acta Crystallogr. C* **40,** 12 (1984).
18. R. J. Gummow, D. C. Liles, and M. M. Thackeray, *Mater. Res. Bull.* **28,** 235 (1993).
19. J. Akimoto, Y. Gotoh, and Y. Osawa, *J. Solid State Chem.* **141,** 298 (1998).
20. J. B. Goodenough, D. G. Wickham, and W. J. Croft, *J. Phys. Chem. Solids* **5,** 107 (1958).
21. A. Rougier, P. Gravereau, and C. Delmas, *J. Electrochem. Soc.* **143,** 1168 (1996).
22. M. Tabuchi, K. Ado, H. Kobayashi, I. Matsubara, H. Kageyama, M. Wakita, S. Tsutsui, S. Nasu, Y. Takeda, C. Masquelier, A. Hirano, and R. Kanno, *J. Solid State Chem.* **141,** 554 (1998).
23. M. Tabuchi, S. Tsutsui, C. Masquelier, R. Kanno, K. Ado, I. Matsubara, S. Nasu, and H. Kageyama, *J. Solid State Chem.* **140,** 159 (1998).
24. M. Tabuchi, S. Tsutsui, H. Kobayashi, H. Sakaebe, C. Masquelier, M. Yonemura, A. Hirano, and R. Kanno, *J. Mater. Chem.* **9,** 199 (1999).